

THS

## This is to certify that the thesis entitled

The Effects of Metallicity on the Brightness of Type Ia Supernovae

presented by

Kimberly L. Dupczak

has been accepted towards fulfillment of the requirements for the

M. S. degree in Astrophysics and Astronomy

Major Professor's Signature

9 May 2008 Date

MSU is an affirmative-action, equal-opportunity employer

## PLACE IN RETURN BOX to remove this checkout from your record. TO AVOID FINES return on or before date due. MAY BE RECALLED with earlier due date if requested.

DATE DUE	DATE DUE	DATE DUE
	-	78
		-

5/08 K:/Proj/Acc&Pres/CIRC/DateDue indd

## THE EFFECTS OF METALLICITY ON THE BRIGHTNESS OF TYPE IA SUPERNOVAE

Ву

Kimberly L. Dupczak

#### A THESIS

Submitted to
Michigan State University
in partial fulfillment of the requirements
for the degree of

MASTER OF SCIENCE

Astrophysics and Astronomy

2008

#### ABSTRACT

## THE EFFECTS OF METALLICITY ON THE BRIGHTNESS OF TYPE IA SUPERNOVAE

By

#### Kimberly L. Dupczak

One of the primary uses of Type Ia supernovae (SNe Ia) is as standard candles (objects of known brightness) to calculate the distance to galaxies. SNe Ia are used as standard candles because they have a peak brightness and lightcurve shape relationship, where the brighter supernovae have broader lightcurves. While this relationship, known as the Phillips' relation, is useful in estimating the peak brightness of SNe Ia, the cause for this relationship is not completely understood. One theory for the observed differences is that the amount of <sup>56</sup>Ni present determines the brightness: the more <sup>56</sup>Ni, the brighter the supernova. This is not the only difference observed among SNe Ia. A dichotomy in where these supernovae occur also exists: the brightest supernovae only occur in galaxies with on-going star formation, while the dimmest ones tend to occur in galaxies with little to no star formation. Several theories exist which attempt to explain these observed relationships, including the possibility of a relationship with the metallicity of the galaxy to the delay time from progenitor formation. In this thesis, I investigate the effects of the galaxies' metallicities on the brightness of the SNe Ia using samples of supernovae and searching for correlations between their change in magnitude over fifteen days vs the metallicity of the host galaxy. The metallicity of the galaxy does not seem to have a strong effect on the brightness of the SNe Ia.

#### TABLE OF CONTENTS

	List	of Figures	iv
1	Intr	oduction: Use of Type Ia Supernovae  Basics of Type Ia Supernovae	1
	1.2	Type Ia Supernovae as Standard Candles	2
	1.3	Cosmological Uses for Type Ia Supernovae	
2	The	Physics of Type Ia Supernovae	5
	2.1	What Defines a Type Ia Supernova?	
		2.1.1 Differences among SNe Ia	
		2.1.2 Relationship between Peak Brightness and <sup>56</sup> Ni	8
		2.1.3 Relationships between Color, Lightcurves, and $M_{\rm Ni}$	11
	2.2	Why Carbon-Oxygen White Dwarfs as the Progenitors?	
		2.2.1 White Dwarfs as the Progenitor	
		2.2.2 Carbon-Oxygen White Dwarfs as the Progenitor	
	2.3	The Single and Double Degenerate Models of Type Ia Supernovae	
		Progenitors	16
		2.3.1 Single-Degenerate System	
		2.3.2 Double-Degenerate System	17
_	Tr4		
3		ting for Correlations	19
	3.1	Background	
	3.2	Data Analysis	
		3.2.1 The Sample	
		3.2.2 Test Used	
		3.2.3 $\Delta m_{15}$ vs $M_B$	
		3.2.4 $\Delta m_{15} \text{ vs } \log \left(\frac{O}{H}\right) + 12 \dots \dots \dots \dots \dots$	22
		3.2.5 $M_{\text{Ni}}$ vs $\log \left(\frac{O}{H}\right) + 12 \dots$	25
4	Con	temporary Studies	27
	4.1	Metallicity Effects	27
	4.2	Two-Component Model	28
		4.2.1 Evidence for the Two-Component Model	
		4.2.2 Evidence against the Two-Component Model	
		4.2.3 Differences between the SNLS and GOODS Surveys	
	4.3	Future Studies	
ים	DT T	OGRAPHY	35
DI	DLI	JURAF II I	ี เรอ

#### LIST OF FIGURES

3.1	Change in Magnitude of Supernova vs. Magnitude of Host Galaxy	23
3.2	Change in Magnitude of Supernova vs. Metallicity of Host Galaxy	24
3.3	Mass of Nickel of Progenitor vs. Metallicity of Host Galaxy	26

## Chapter 1

Introduction: Use of Type Ia

Supernovae

#### 1.1 Basics of Type Ia Supernovae

Spectroscopically, two types of supernovae exist: Type I supernovae that do not contain hydrogen in their spectra, and Type II supernovae that do contain hydrogen in their spectra. These two types are then further broken down into sub-classes based on the features in their spectra. Type Ia supernovae (SNe Ia) lack Balmer hydrogen lines and has strong SiII absorption lines in their spectra. SNe Ia are thought to be the explosion of C-O white dwarfs whose masses are near the Chandrasekhar mass limit, which is the maximum mass that can be supported by electron degeneracy pressure. White dwarfs are essentially the core of a star that has blown off its outer layers. While thermonuclear fusion generally does not occur in the white dwarf, it can be reignited if the white dwarf accretes enough matter on the outside layers to increase the pressure, and thus the temperature, inside the core. This ignition occurs as the star approaches the Chandrasekhar mass limit of  $1.4~M_{\odot}$  (Iben & Tutukov,

#### 1.2 Type Ia Supernovae as Standard Candles

Since SNe Ia are thought to be the result of the same physical process, all of the supernovae should have approximately the same peak brightness. When the absolute brightness of an object is known, it is possible to find the distance to it after measuring the apparent brightness. While the peak brightnesses of the supernovae is not exactly the same for every event, the spread in their intrinsic brightness is relativley small. Locally, the dispersion is peak magnitude is  $\sim 0.5$  mag in B and V. When including more distant SNe Ia in the sample, subluminous events broaden this dispersion to  $\sim 1$  mag in B and V (Sullivan et al., 2006).

Other advantages SNe Ia have as distance indicators include where they occur and their lightcurve shape. SNe Ia occur in both spiral and elliptical galaxies, thus one is not limited by galaxy type when determining the distance to the galaxy (Colgate, 1979). The homogeneity of the lightcurve shape also puts SNe Ia at an advantage as a standard candle. The lightcurve of an SNe Ia is distinguishable from other types of supernovae. Thus, one can identify a SNe Ia even if it not observed until sometime after peak brightness. The observed lightcurve can also be fitted to templates so that the peak brightness of the SNe Ia can be determined (Riess et al., 1995).

#### 1.3 Cosmological Uses for Type Ia Supernovae

SNe Ia can also be used to determine the Hubble constant  $H_0$  and the cosmological constants  $\Omega_M$  and  $\Omega_\Lambda$ .  $H_0$  relates the recessional velocity of an object to its distance from us,  $v = H_0 d$ . Thus, the further an object is from us in space, the faster it is moving away from us.  $\Omega_M$  is defined as the average density of matter over the whole universe divided by the critical density, where the critical density is the energy needed to counteract  $H_0$ .  $\Omega_\Lambda$  is defined as the average vacuum energy density over the whole universe divided by the critical density. Colgate (1979) suggested using SNe Ia as a way to measure  $H_0$  with greater accuracy than other standard candles. The measured luminosity is dependent on the redshift and  $H_0$ . Thus, if the rest frame luminosity is known, one can constrain  $H_0$  based on the measured luminosity and redshift. Goobar & Perlmutter (1995) also advocated the use of standard candles as a way to measure  $\Omega_M$  and  $\Omega_\Lambda$ . If  $\Omega_\Lambda$  is not zero, then the magnitude-redshift measurement is sensitive to  $\Omega_M$  and  $\Omega_\Lambda$  through the luminosity distance  $D_L$ . The magnitude-redshift distance is defined as

$$m = M + 5 \log[D_L(z; \Omega_M, \Omega_{\Lambda})] + K + 25, \tag{1.1}$$

where K is the K-correction applied to the object. The K-correction is a correction of an object's magnitude through a filter so that the measurements can be compared to the object's magnitude in the rest frame. The luminosity distance  $D_L$  is defined as

$$D_L(z;\Omega_M,\Omega_{\Lambda}) = \frac{1+z}{H_0\sqrt{\kappa}} S\left(\sqrt{\kappa} \int_0^z [(1+z')^2 (1+\Omega_M z') - z'(2+z')\Omega_{\Lambda}]^{-1/2} dz'\right),$$
(1.2)

where

- if  $\Omega_M + \Omega_{\Lambda} < 1$ ,  $S(x) = \sin(x)$ ,  $\kappa = 1 \Omega_M \Omega_{\Lambda}$ , and the universe is defined as closed
- if  $\Omega_M + \Omega_{\Lambda} > 1$ ,  $S(x) = \sinh(x)$ ,  $\kappa = 1 \Omega_M \Omega_{\Lambda}$ , and the universe is defined as open
- if  $\Omega_M + \Omega_{\Lambda} = 1$ , S(x) = x,  $\kappa = 1$ , and the universe is defined as flat.

Using these two equations, one can predict the apparant magnitude of a standard candle at a given redshift z based on the pair of  $\Omega_M$  and  $\Omega_\Lambda$ . When actual apparent magnitude measurements of a standard candle are made at a specific z, one can narrow the ranges of  $\Omega_M$  and  $\Omega_\Lambda$ . Two such measurements at different redshifts can define two ranges of possible  $\Omega_M$  and  $\Omega_\Lambda$  that cross in a more narrowly constrained region. In the special case of a flat universe, which is the universe predicted by inflationary theories, the apparent magnitude as a function of z is extremely sensitive to  $\Omega_\Lambda$ . A measurement of a standard candle at z=1 would strongly constrain  $\Omega_\Lambda$  and test inflationary theories.

Perlmutter et al. (1999) studied 42 SNe Ia at z=0.18-0.83 and found that a flat universe with  $\Omega_{\Lambda}=0$  is strongly inconsistent with the data. Instead, if the simplest inflationary models were correct and the universe was flat, then there was a significant, positive  $\Omega_{\Lambda}$ . Therefore, the universe could be flat or there was a small or no  $\Omega_{\Lambda}$ . Perlmutter et al. found that if the universe was flat, then  $\Omega_{M}=0.28^{+0.09}_{-0.08}$ , which indicated that  $\Omega_{\Lambda}\approx 0.72$ . This value of  $\Omega_{\Lambda}$  further indicated that the cosmological constant  $\Lambda$ , which is related to  $\Omega_{\Lambda}$  by  $\Omega_{\Lambda}\equiv \Lambda/3H_{0}^{2}$ , was a significant constituent of the energy density of the universe. Results from the Wilkinson Microwave Anisotropy Probe (WMAP) confirm these values for  $\Omega_{M}$  and  $\Omega_{\Lambda}$  (Tegmark et al., 2004).

### Chapter 2

## The Physics of Type Ia Supernovae

#### 2.1 What Defines a Type Ia Supernova?

Historically, supernovae were divided into two classes, Type I and Type II. Supernovae classified as Type I do not contain Balmer hydrogen lines in their optical spectra, while the supernovae classified as Type II do (Doggett & Branch, 1985). If the spectrum of the supernova was unavailable, then the supernova could be classified by the shape of its lightcurve. The lightcurve of a Type I supernova generally has the following characteristics: a sharp change in the rate of decline occurs about 30 days after maximum brightness with the fast, early decline ending and a slower, final decline beginning; at this point, the change in magnitude is about 2.7 (Barbon et al., 1973).

Some spectra and lightcurves of supernova classified as Type I did not have all of these characteristics. In the mid-80s, astronomers divided Type I supernovae into

two classes: Type Ia have the above mentioned characteristics in their spectra and lightcurves, and Type Ib do not. The spectra of Type Ia and Type Ib are initially very different. In a Type Ia, the optical spectrum at maximum light contains a strong absorption feature of SiII  $\lambda$ 6355 and features which are interpreted as overlapping P-Cygni profiles of neutral and singly ionized intermediate-mass elements, such as oxygen, silicon, and calcium. (A P-Cygni profile arises when a star has a hot, stellar wind. The spectrum from such a star contains blue-shifted absorption features, which arises from material directly along the line of sight moving through the wind, and red-shifted emission features, which arises from radiation scattering off of the wind on the back and sides.) The outer layers of the ejecta are mainly composed of these intermediate mass elements. Permitted FeII lines begin to dominate the spectra  $\sim 2$  weeks after maximum light. Finally, about one month after maximum light, features from the intermediate-mass elements disappear and forbidden FeII, FeIII, and CoIII features become dominant (Branch, 1986; Hillebrandt & Niemeyer, 2000). On the other hand, the optical spectrum of a Type Ib supernova lacks the intermediate-mass features and the SiII  $\lambda 6355$  absorption feature at maximum light. Instead, the spectrum is dominated by the FeII blends (Branch, 1986).

The lightcurves of Type Ia and Ib supernovae can also be used to distinguish between the two, especially in the infrared. The infrared lightcurve of a Type Ia supernova displays an absorption dip  $\sim 20$  days after maximum light and a secondary peak  $\sim 30$  days after maximum light. On the other hand, a Type Ib light curve does not contain these features. Instead, the lightcurve falls monotonically after maximum light (Gaskell et al., 1986).

#### 2.1.1 Differences among SNe Ia

SNe Ia are thought to be the explosion of CO white dwarfs that are approaching the Chandrasekhar mass limit of  $1.4M_{\odot}$ . Since the SNe Ia are caused by the same process, they should all achieve the same peak brightness (Iben & Tutukov, 1984; Woosley et al., 1986; Phillips, 1993). Observations of several supernovae, however, questioned the apparent homogeneous nature of SNe Ia. Leibundgut et al. (1993) reported that SN 1991bg was an unusually dim SNe Ia. Branch & Miller (1993) confirmed that this was an intrinsically dim supernova, noting that its lightcurve was fast-declining.

The observation of the dim supernovae having a faster declining lightcurve supported the peak brightness – initial decline rate correlation claimed by Pskovskii (1977, 1984). To measure the initial decline rate of the lightcurve, Pskovskii (1984) defined a slope parameter  $\beta$  as the mean rate of decline of the B-band light curve between the peak brightness and the bend in the light curve, which usually occurs 25-30 days later. Phillips (1993) employed a much simpler method. Instead of measuring the rate of decline, Phillips measured the total amount in magnitudes that the light curve decayed from peak brightness during some specified period following peak brightness. A time interval of 15 days showed the greatest discrimination, becoming known as the  $\Delta m_{15}$  parameter. SNe Ia with low  $\Delta m_{15}$  values are brighter, while SNe Ia with high  $\Delta m_{15}$  are dimmer.

Related to the  $\Delta m_{15}$  parameter is the stretch factor of the supernova lightcurve (Perlmutter et al., 1997). The lightcurves of SNe Ia have the same general shape - the rate of decline affects how wide the lightcurve is. When working with the stretch of the lightcurve, the time axis of a template curve is multiplied by a scale factor to fit the observed data. This allows for an estimation of the peak brightness of the

supernova.

#### 2.1.2 Relationship between Peak Brightness and <sup>56</sup>Ni

Colgate & McKee (1969) found that a large mass fraction of <sup>56</sup>Ni was critical to explain the observed lightcurves. The rate of the radioactive heating within the supernova is determined by the following equation:

$$S = -q_{\text{Ni}\to\text{Co}} \frac{dN_{\text{Ni}}}{dt} + q_{\text{Co}\to\text{Fe}} \frac{dN_{\text{Co}}}{dt}, \qquad (2.1)$$

where q is the energy factor for the reaction. The change in abundance of  $^{56}$ Ni and  $^{56}$ Co are denoted by:

$$\frac{dN_{\text{Ni}}}{dt} = N_0 e^{-\gamma_{\text{Ni}} - \text{Co}} \tag{2.2}$$

and

$$\frac{dN_{\text{Co}}}{dt} = \frac{N_0}{\gamma_{\text{Ni}} - \gamma_{\text{Co}}} (\gamma_{\text{Co}} e^{-\gamma_{\text{Ni}} t} - \gamma_{\text{Ni}} e^{-\gamma_{\text{Co}} t} + N_0), \tag{2.3}$$

where  $\gamma$  is the inverse of the half-life of the element, and  $N_0$  is the original amount of <sup>56</sup>Ni. After substituting  $\gamma_{\text{Co}} = (111 \text{ d})^{-1}$ ,  $\gamma_{\text{Ni}} = (8.7 \text{ d})^{-1}$ ,  $q_{\text{Co}} = 3426.1 \text{ keV}$ , and  $q_{\text{Ni}} = 4566.0 \text{ keV}$ , we get

$$S(t) = \left[7.79 \times 10^{43} e^{-t/8.7} + 1.41 \times 10^{43} \left(e^{-t/111} - e^{-t/8.7}\right)\right] \text{ ergs s}^{-1} M_{\odot}^{-1}$$
 (2.4)

for t in days. The decay process  $^{56}\text{Ni} \rightarrow ^{56}\text{Co}$  supplies the radiant energy leading up to the maximum brightness, while the decay process  $^{56}\text{Co} \rightarrow ^{56}\text{Fe}$  contributes to the exponential light-decay after peak brightness.

Arnett (1982) expanded on this model. Based on Arnett's models, the peak brightness is a function of <sup>56</sup>Ni mass: the more <sup>56</sup>Ni synthesized, the brighter the

supernova, or

$$M_{\rm Ni} = \frac{L_{\rm Bol}}{\gamma S(t_R)},\tag{2.5}$$

where  $L_{\rm Bol}$  is the bolometric luminosity,  $\gamma$  is a scaling factor, and  $S(t_R)$  is the rate of radioactive heating given in 2.4 evaluated at the risetime (time to reach maximum brightness) in days. Substituting in  $L_{\rm Bol} = L_{\odot}10^{0.4(4.75-M_{\rm Bol})}$ , the bolometric magnitude  $M_{\rm Bol} = -19.31 + 0.18 - 1.52(s-1)$ , and  $\gamma = 1.2$  (Nugent et al., 1995; Howell et al., 2006) into the above equation, and evaluating it at  $t_R = 19.5 \times s$  (Astier et al., 2006), we get

$$M_{\text{Ni}} = \frac{1.15e^{1.4(s-1)}}{7.79e^{-2.23s} + 1.41(e^{-0.176s} - e^{-2.23s})},$$
 (2.6)

where s is the stretch factor for the timescale, and  $t_R = 19.5$  is the risetime in days for the standard model. Evaluating at s = 1, which is the stretch factor for the standard template, yields  $M_{\rm Ni} = 0.615~M_{\odot}$ . While the rise to peak brightness is driven by the decay of  $^{56}{\rm Ni}$ , the energy released from the decay of  $^{56}{\rm Co}$  to  $^{56}{\rm Fe}$  exceeds that of  $^{56}{\rm Ni}$  at approximately the time of maximum brightness. This is due to the fact that it takes time for this energy to diffuse out of the star. Thus the contribution of the  $^{56}{\rm Co}$  energy to the shape of the lightcurve is seen after the peak brightness.

Further models by Arnett (1999) demonstrated under what conditions one would then have the observed Phillips relation. Arnett defined the bolometric luminosity of the supernova as

$$L_{\text{Bol}} = \epsilon_{\text{Ni}} M_{\text{Ni}} \Lambda(x, y). \tag{2.7}$$

Here,  $\epsilon_{\rm Ni}$  is the energy of radioactive decay of  $^{56}{\rm Ni}$  per unit mass, divided by the mean lifetime of  $^{56}{\rm Ni}$   $\tau_{\rm Ni}$ , and  $\Lambda(x,y)$  is the dimensionless function

$$\Lambda(x,y) = e^{-x^2} \int_0^x e^{-2zy+z^2} 2z dz. \tag{2.8}$$

Here,  $x = t/\tau_m$  and  $y = \sqrt{2\tau_h\tau_0}/(2\tau_{\rm Ni})$ , where  $\tau_m$  is the effective escape time,  $\tau_h$  is the expansion time, and  $\tau_0$  is the diffusion time. To get the observed Phillips' relation, Arnett determined how  $M({\rm Ni})$  changed with y. Assuming that  $\tau_0 = R^2 \rho \kappa/c$ , where R is the radius,  $\rho$  is the average density,  $\kappa$  is a constant opacity, and c is the speed of light, then

$$y = \frac{(2\tau_h \tau_0)^{1/2}}{2\tau_{Ni}}$$

$$\propto (\tau_h \tau_0)^{1/2}$$

$$\propto \left(\tau_h \frac{R^2 \rho \kappa}{c}\right)^{1/2}$$

After substituting in  $\rho \propto M/R^3$ , where M is the total mass, and  $\tau_h = R/v_{sc}$ , where  $v_{sc}$  is a characteristic velocity scale, we find

$$y \propto \left(rac{M^3}{v_{sc}}
ight)^{1/2}.$$

The total energy of the supernova  $E_{\rm SN}$  is

$$E_{\mathrm{SN}} = \frac{1}{2} M \left\langle v_{sc}^2 \right\rangle.$$

Thus

$$y \propto \left(\frac{M^3}{E_{\rm SN}}\right)^{1/4}.\tag{2.9}$$

Using the above proportion we get

$$L = \epsilon_{
m Ni} M_{
m Ni} \Lambda_{
m max}$$
 $\propto M_{
m Ni} \Lambda_{
m max}$ 
 $\propto M_{
m Ni} / y$ 
 $\propto y^3$ 

where  $\Lambda_{\text{max}} \propto 1/y$  and  $E \gg 0.7 \times 10^{51}$  ergs (Arnett, 1982, 1999). This equation gives the Phillips' relation of brighter SNe Ia have broader lightcurves.

However, if the  $^{56}$ Ni is distributed as a central sphere of pure  $^{56}$ Ni, then the average distance of the  $^{56}$ Ni to the surface increases with  $M_{\rm Ni}$ , and so does the probability of energy leakage from gamma and x-ray emission. This leakage changes the lightcurve shape, and thus the Phillips relation may be destroyed. Alternatively, if the  $^{56}$ Ni distribution is not a strong function of the  $M_{\rm Ni}$  at a time several days after explosion, then the Phillips' relation is observed (Arnett, 1999, and references therein).

#### 2.1.3 Relationships between Color, Lightcurves, and $M_{Ni}$

#### Color and $M_{Ni}$

Since there is a correlation with the lightcurve shape, and thus  $\Delta m_{15}$ , and  $M_{\rm Ni}$ , one can estimate the amount of  $^{56}{\rm Ni}$  in the progenitor. Kasen & Woosley (2007) created models which estimated the amount of  $^{56}{\rm Ni}$  based on the  $\Delta m_{15}$ . Within these models, Kasen and Woosley discovered that  $M_{\rm Ni}$  had a greater effect on the color and spectroscopic evolutions of the models. The faster-declining (dimmer) SNe Ia were redder 15 days later. This color evolution was due to the impact of iron group lines on post-maximum spectra: dimmer SNe Ia have a more rapid development of Fe II/Co II lines. Thus, for a given  $M_{\rm Ni}$ , enhancing the iron group abundance in the outer layers of the ejecta increased the B-band decline rate, producing dimmer supernovae.

#### Lightcurve and $M_{Ni}$

How well the  $M_{\rm Ni}$  is mixed within the progenitor has an effect on the shape of the observed lightcurve, specifically in the infrared. Near-infrared observations, such as those with the I- through K-bands, show that the supernovae have a secondary maximum roughly 20-30 days after the primary maximum. Kasen (2006) demonstrated that these double maxima in SNe Ia are directly related to the ionization evolution of the iron group elements, such as  $^{56}$ Ni, in the supernovae ejecta. Specifically, the NIR emissivity of iron/cobalt increases sharply at a temperature  $T \approx 7000 K$ . The cooling of the iron rich layers of ejecta to this temperature is accomplanied by a sudden increase in emission at NIR wavelengths.

Kasen (2006) also demonstrated the dependence of the secondary maximum on the mixing of the  $M_{\rm Ni}$  in the progenitor. If the progenitor has a thoroughly mixed composition, then the first and second maxima are indistinguishable in every band. If the composition is more stratified, then the two maxima are more distinguishable from each other. Thus, the appearance of the maxima is useful in constraining the exact degree of mixing within the progenitor. The  $M_{\rm Ni}$  also has an effect on the appearance of the second maximum. In the visible bands, the more  $M_{\rm Ni}$ , the brighter the supernova (Arnett, 1982, 1999), thus the more pronounced the first maximum. This effect can also be seen in the second maximum in the NIR bands.

# 2.2 Why Carbon-Oxygen White Dwarfs as the Progenitors?

#### 2.2.1 White Dwarfs as the Progenitor

The features observed in the spectra and lightcurves of Type Ia supernovae indicate that a compact object is the progenitor of these phenomena. The change in the spectrum from being dominated by intermediate-mass elements to FeII approximately two weeks after maximum light indicates that the supernovae are caused by the thermonuclear explosions of compact objects, such as the cores of main-sequence stars with masses 6-8  $\ensuremath{M_{\odot}}$  or white dwarfs. The presence of some UV flux, the width of the peak of the early lightcurve, and the fact that models of the radioactive decay of  $^{56}\text{Ni} \rightarrow ^{56}\text{Co} \rightarrow ^{56}\text{Fe}$  fit the observed emission well, support the idea that the progenitor is a star with a radius of less than 10,000 km (Hillebrandt & Niemeyer, 2000). The observation of <sup>56</sup>Fe and the radioactive decay products of <sup>56</sup>Ni and <sup>56</sup>Co in the spectrum of the supernova supports this hypothesis. The velocities inferred from spectral measurements and the total energy emitted from the supernovae agree with the calculations one would obtain by converting a fraction of the mass of a white dwarf to <sup>56</sup>Fe or <sup>56</sup>Ni. The degenerative nature of white dwarfs guarantees that a nuclear runaway reaction will convert a substantial fraction of the mass of a white dwarf on a short timescale, with the resulting lightcurve being generated by the decay of the radioactive species in the reaction (Woosley et al., 1986).

Other evidence for white dwarfs being the progenitors include the location of the supernovae. Unlike core-collapse supernovae, SNe Ia occur in all types of galaxies. This implies that the progenitor is an evolved star, such as a white dwarf. SNe Ia are not associated with HII regions in spiral galaxies, which are areas of active star

formation (van Dyk, 1992), and they also occur in elliptical galaxies, which has little to no active star formation (Turatto et al., 1994). Both observations imply that the supernovae do not result from the core collapse of stars with masses greater than 8  $M_{\odot}$  (Branch et al., 1995).

#### 2.2.2 Carbon-Oxygen White Dwarfs as the Progenitor

Astronomers further suspect that white dwarfs composed of carbon and oxygen, as opposed to helium or oxygen, neon, and magnesium, are the progenitors of SNe Ia. While He white dwarfs can be formed from stars in a binary system and can explode, the ejected matter does not match the observations of the spectra of SNe Ia. Woosley et al. (1986) have shown that the spectrum of He white dwarf explosion severely disagrees with the observed spectrum of SNe Ia at early and late times. For example, the helium white dwarf models do not contain any appreciable abundance of silicon or sulfur, two elements which have high abundances in the spectra of SNe Ia. Also, the high velocities associated with the explosion would cause broader and more highly shifted emission lines. The models in Woosley et al. (1986) indicate that the higher velocities would cause broader emission lines of iron than what is observed. Other consequences of the higher velocities include very high ionization stages of iron at later times, which is in disagreement with observations.

O-Ne-Mg white dwarfs are also possible progenitors for SNe Ia. However, if the O-Ne-Mg white dwarf does approach its Chandrasekhar mass limit, it is expected to collapse and form a neutron star, not explode into a supernova. Miyaji et al. (1980) have shown that as the O-Ne-Mg white dwarf accretes matter from a companion star, electrons capture onto  $^{24}$ Mg and  $^{24}$ Na first, then onto  $^{20}$ Ne and  $^{20}$ F later. This causes  $^{20}$ Ne and  $^{16}$ O to explosively ignite at a central density of  $\rho_c > 2 \times 10^{10}$  g cm $^{-3}$ . At this high of a density, the fast electron captures onto the nuclear statistical

equilibrium material quickly reduces the Chandrasekhar mass limit to less than that of the actual mass of the core, inducing gravitational collapse. Gutierrez et al. (1996) demonstrated that if convective mixing occurs, then the range of densities for explosive ignition is  $(9.74-21.2)\times 10^9$  g cm<sup>-3</sup>. These values lie above the minimum ignition density for gravitational collapse:  $9\times 10^9$  g cm<sup>-3</sup>. Thus, unless the O-Ne-Mg white dwarf ignites <sup>24</sup>Ne before the electron captures onto <sup>24</sup>Mg and <sup>24</sup>Na, the core will collapse to nuclear matter densities. In the case of a mass-accreting white dwarf, the result is a non-explosive collapse to a neutron star.

Models of carbon-oxygen white dwarfs, on the other hand, best reproduce the observed conditions described in the previous section (Woosley et al., 1986; Hillebrandt & Niemeyer, 2000). The element <sup>56</sup>Ni is the dominant product of nucleosynthesis starting from fuel with equal numbers of protons and neutrons, like <sup>12</sup>C and <sup>16</sup>O (Woosley et al., 2007). Also, unlike the O-Ne-Mg white dwarfs which will gravitationally collapse as it approaches its Chandrasekhar mass limit, a CO white dwarf will undergo carbon deflagration in its core as it approaches its Chandrasekhar mass limit, as long as the mass accretion rate is high enough so that matter can accumulate on the white dwarf uninterrupted by mass ejection (Taam, 1980). Based on models, carbon deflagration naturally accounts for the existence of intermediate mass elements Ca through O in the outer layers of the white dwarf. These models also show that the ejecta contains substantial amounts of Ca through Si and produce Si peak elements, which are consistent with observations. Finally, the carbon deflagration model predicts complete disruption of the progenitor, which is consistent with observations (Nomoto et al., 1984).

# 2.3 The Single and Double Degenerate Models of Type Ia Supernovae Progenitors

Most astronomers agree that while a CO white dwarf is the progenitor of a SNe Ia, the white dwarf must be in a binary system in order to accrete enough matter to approach the Chandrasekhar mass limit in order to explode. The white dwarfs accrete mass from the companions until they explode (Branch et al., 1995, and references therein). Two of the most common models are the single degenerate (SD) system, where a non-degenerate companion, eg, a red giant, orbits the white dwarf, and a double-degenerate (DD) system, where two white dwarfs orbit each other (Nomoto, 1982; Iben & Tutukov, 1984).

#### 2.3.1 Single-Degenerate System

In the SD system, a non-degenerate companion star begins to expand over its Roche lobe (limit where orbiting material is gravitationally bound to the star) and accretes matter onto the white dwarf. When enough hydrogen-rich material is accreted onto the surface of the white dwarf, hydrogen-shell burning begins. If the rate of accretion is rapid, then burning is stable and the resultant helium settles onto the surface of the white dwarf. Eventually, if enough mass accretes rapidly enough, the pressure increases enough for carbon fusion to occur in the core. While the pressure in the core increases slowly, the temperature continues to rise, which increases the fusion rate. This in turn leads to a runaway reaction, and the white dwarf explodes due to the carbon deflagration (Nomoto, 1982). This central carbon-deflagration of the white dwarf would produce iron and traces of elements from carbon to silicon, which matches observations (Matteucci et al., 2006). The observed diversity in SNe Ia

would be caused by differences in the ejected  $M_{\rm Ni}$  (Branch, 2001).

However, there is a narrow range of permitted values for steady mass accretion rate onto the white dwarf. If the accretion rate is not steady, then the white dwarf could undergo a nova explosion, where it expels its outer layers but does not destroy itself, and mass loss. Because of this, the white dwarf would never reach the Chandrasekhar mass limit (Matteucci et al., 2006). Also, simulations of this scenario imply the presence of low-velocity  $H\alpha$ -emission in the late-time spectra of the supernovae since a portion of the companion's envelope gets mixed with the ejecta. While the  $H\alpha$ -emission has not been detected, it rarely has been sought (Leonard, 2007).

#### 2.3.2 Double-Degenerate System

In the DD system, two CO white dwarfs coalesce until their combined mass exceeds the Chandrasekhar mass limit. For degenerate white dwarfs, the larger the mass, the smaller the radius of the star. Thus, the lower mass white dwarf will fill its Roche lobe first. This matter is accreted onto the higher mass white dwarf. However, the matter does not settle onto the accreting white dwarf immediately. Instead, matter first forms a disk around the accreting white dwarf. The disk formation may be a response to conserve angular momentum. This disk will then cause the accreting white dwarf to expand its radius until it is at least as large as that given by the Eddington luminosity, or the maximum luminosity a star can have before the radiation pressure exceeds the gravitational force. Eventually, the accreting white dwarf will be able to accept the matter from the disk surrounding it. When enough matter builds up, then like the SD system, the white dwarf will explode due to carbon deflagration (Iben & Tutukov, 1984).

While the DD scenario would explain the lack of hydrogen observed in the spectra, there are several problems with it observationally and theoretically. Observationally, of the  $\sim 120$  DD systems known, none of them are in excess of Chandrasekhar mass limit. Theoretically, the largest mergers would most likely lead to a collapse to a neutron star rather than a thermonuclear explosion (Leonard, 2007). However, Piersanti et al. (2003) found that if the mass accretion rate  $\dot{M}$  and initial angular momentum  $\omega_0$  of the accreting white dwarf is low enough, then the star can accrete enough matter to approach  $1.4M_{\odot}$ . Otherwise, if  $\dot{M}$  and  $\omega_0$  are too high, then the accreting star becomes gravitationally unbound and no matter can be added to it.

## Chapter 3

## **Testing for Correlations**

#### 3.1 Background

Observations have shown that a disparity exists between the locations of dim and bright supernovae. Dimmer supernovae tended to occur in galaxies with zero-to-low star formation ("passive"); brighter supernovae in galaxies with high star formation ("active")(Hamuy et al., 2000; Hachinger et al., 2006). The passive galaxies tend to be older elliptical galaxies with higher metallicity. No bright supernovae have been observed in these types of galaxies. The active galaxies tend to be young spiral galaxies with lower metallicity. Unlike the passive galaxies, active galaxies could host dimmer supernovae (Hamuy et al., 2000; Gallagher et al., 2005; Hachinger et al., 2006).

Two galactic properties that could affect the peak brightness of the supernovae within the galaxy are the metallicity of the galaxy and the age of the galaxy. Hamuy et al. (2000) pointed out that the brightest supernovae occurred in the least luminous galaxies. These galaxies also tend to be bluer in color. The galaxies are less

luminous because they are less massive, and therefore not able to retain the metals as efficiently. If there are less metals in the progenitor, the energy will be able to radiate outwards more efficiently, thereby reducing diffusion time and leading to a brighter supernova. Thus, metallicity of the galaxy could be a factor of variations in peak brightness. On the other hand, since these galaxies are bluer, they are younger. Thus, age could be a factor. However, one characteristic could mask the other's importance in determining the brightness of the supernova. For example, younger galaxies tend not to have a very high metallicity because the stars within the galaxy have not had the time to produce the metals. Thus, it is important to separate the effects of one factor over the other.

Since this difference in location of the supernovae does exist, we wanted to see if the metallicity of the progenitor was a factor in the brightness of the supernova. Timmes et al. (2003) showed that the metallicity of the progenitor would affect the amount of <sup>56</sup>Ni: the higher the metallicity, the lower the amount of <sup>56</sup>Ni. When testing for a correlation between the metallicity of the progenitor and the brightness of the supernova, we had to assume that the metallicity of the progenitor was similar to the average metallicity of the galaxy. It is impossible to measure the individual metallicity of the progenitor. With a large enough sample, a trend in the metallicity ought to be discernable.

#### 3.2 Data Analysis

#### 3.2.1 The Sample

The sample of the supernovae came from Hachinger et al. (2006) and Gallagher et al. (2005) papers. From these papers I gathered the supernova names,  $\Delta m_{15}$ 

parameter and corresponding error, and host galaxy name. The  $\Delta m_{15}$  parameter and corresponding error were important because this indicates the brightness of the supernova: brighter supernovae have smaller  $\Delta m_{15}$  values. However, information about the properties of the host galaxy, such as absolute brightness and metallicity, was usually found from other sources or calculated, which is described below. Following the criteria listed in Reindl et al. (2005), I removed any supernovae that were considered "non-standard." The non-standard criteria included those supernovae that were very overluminous and very underluminous. The overluminous ones had peculiar spectra, while the underluminous ones were very red and had very fast decline rates,  $\Delta m_{15} \approx 1.9$ .

#### 3.2.2 Test Used

To determine any correlations among the variable, we used the Spearman correlation test, which assesses how well an arbitrary monotonic function could describe the relationship between two variables, without making any assumptions about the frequency distribution of the variables. In order to do this, the two variable arrays are ranked from lowest to highest. The test then compares the ranks of the two corresponding variables and returns a value  $\rho$  between -1 and 1. The value  $\rho$  is determined by

$$\rho = 1 - \frac{6\sum d_i^2}{n(n^2 - 1)} \tag{3.1}$$

where d is the difference between the two corresponding variables and n is the number of pairs of values. The closer the number is to -1 or 1, the stronger the correlation between the two variables.

#### 3.2.3 $\Delta m_{15}$ vs $M_B$

In the beginning, as a proxy for the metallicity of the galaxy, we used the absolute brightness  $M_B$  of the galaxy, which is generally more readily available than the metallicity. Since there is a tighter correlation between  $M_B$  and metallicity of a spiral galaxy (Henry & Worthey, 1999; Pilyugin et al., 2004), I only looked at the supernovae that occurred in spiral galaxies. The values for  $\Delta m_{15}$  and  $M_B$  came from the above papers. If the host galaxy did not have an  $M_B$  listed in the paper, then the value came from the NASA/IPAC Extragalactic Database. After plotting the  $\Delta m_{15}$  of the supernovae vs. the  $M_B$  of the galaxy, I ran the Spearman correlation test. With  $\rho = -0.36$ , the test did not reveal a significant correlation between  $\Delta m_{15}$  and  $M_B$  at the 95% confidence level.

### **3.2.4** $\Delta m_{15}$ vs $\log \left(\frac{O}{H}\right) + 12$

Later, I followed a procedure outlined in Tremonti et al. (2004) to calculate the metallicity of the galaxy using its  $M_B$ . Based on the spectra of 53,000 star-forming galaxies within the Sloan Digital Sky Survey (SDSS), the procedure calculates the metallicity of the galaxy using strong optical nebular lines, which is an improvement over methods that rely on single line ratios. The advantages are: the S/N in emission lines can greatly exceed the S/N in the continuum; the calculations are free of uncertainties due to age and  $\alpha$ -enhancement; easier to interpret the results because they reflect present-day metal abundance rather than the luminosity-weighted average of previous stellar generations. The disadvantage is that this method is limited to galaxies with on-going star formation.

Tremonti et al. (2004) calculated the metallicity as  $\log \left(\frac{O}{H}\right) + 12$ , where  $\frac{O}{H}$  is the ratio of the oxygen abundance to the hydrogen abundance in the galaxy. To esti-

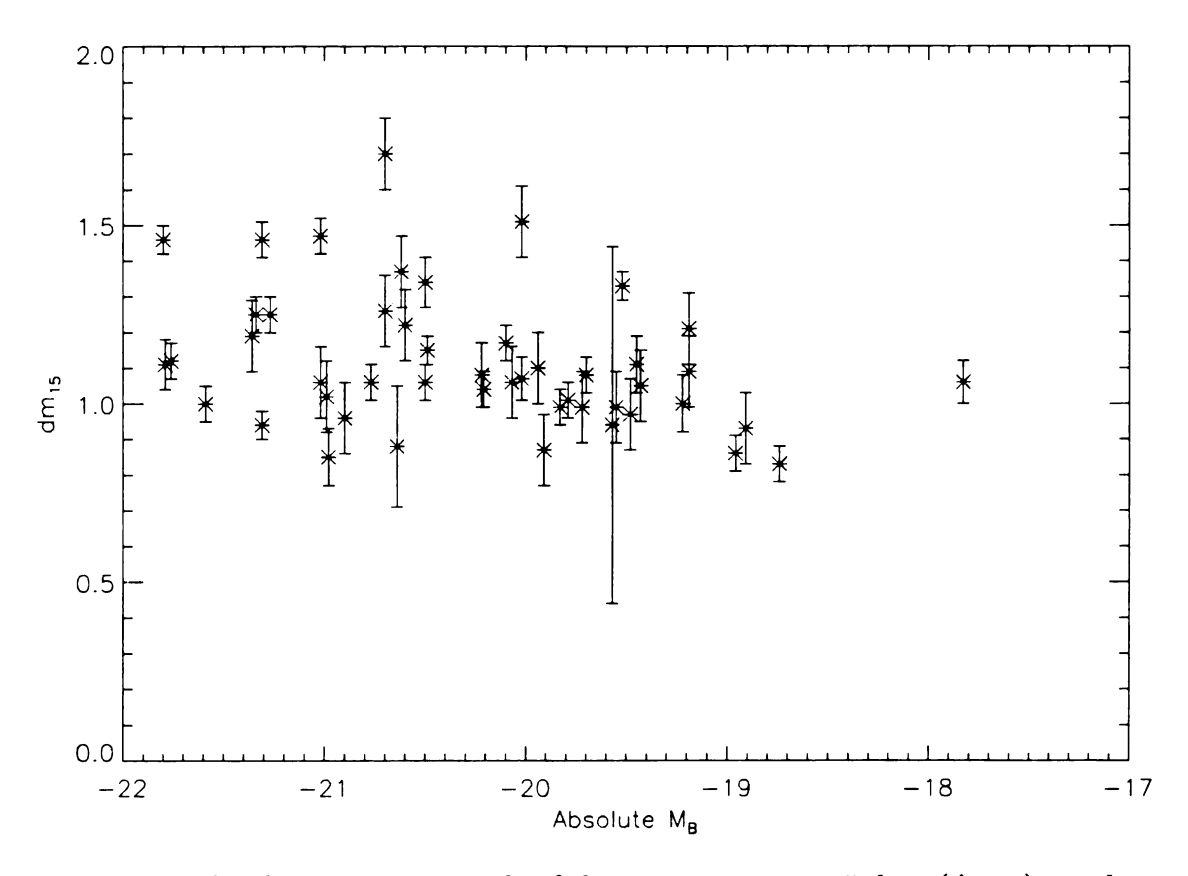


Figure 3.1: The change in magnitude of the supernova over 15 days  $(\Delta m_{15})$  vs. the absolute magnitude of the host galaxy  $(M_B)$ . A Spearman correlation test on the data indicated that there is a very weak correlation between  $M_B$  of the host galaxy and  $\Delta m_{15}$  of the supernova.

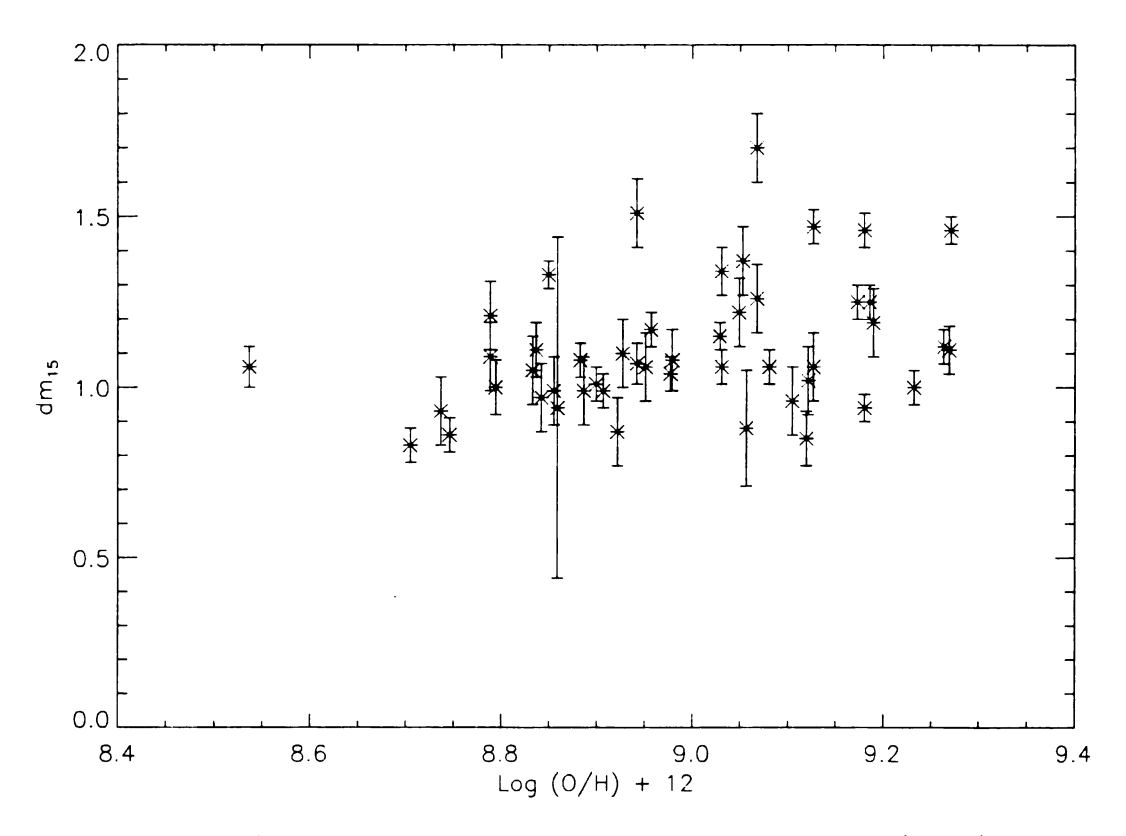


Figure 3.2: The change in magnitude over 15 days of the supernova ( $\Delta m_{15}$ ) vs the metallicity of the host galaxy (log  $\left(\frac{O}{H}\right) + 12$ ). A Spearman correlation test indicated that there was no significant relationship between the metallicity of the host galaxy and the brightness of the supernova.

mate the metallicities of the galaxies in their sample, they simultaneously fitted the most prominent emission lines ([OII], H $\beta$ , [OIII], H $\alpha$ , [NII], and [SII]) with a model designed for the interpretation of integrated galaxy spectra. Based on the metallicities and  $M_B$  of the galaxies, they found that  $\log\left(\frac{O}{H}\right) + 12 = -0.185(\pm 0.001)M_B + 5.238(\pm 0.0018)$ . I converted  $M_B$  of the host galaxies to  $\log\left(\frac{O}{H}\right) + 12$  so that I could directly compare  $\Delta m_{15}$  to the metallicity of the galaxy. After obtaining the metallicity of the galaxies from our sample using this equation, I plotted  $\Delta m_{15}$  vs. the results. I also performed the Spearman correlation test on the results as a check. Since  $M_B$  and  $\log\left(\frac{O}{H}\right) + 12$  are linearly related, the magnitude of the Spearman correlation coefficient should be the same, and it was at  $\rho = 0.36$ .

#### **3.2.5** $M_{\text{Ni}}$ vs $\log \left( \frac{\text{O}}{\text{H}} \right) + 12$

As a final test, I calculated the  $M_{\rm Ni}$  of the progenitor following the procedure outlined in Kasen & Woosley (2007). This procedure calculates the  $M_{\rm Ni}$  based on the  $\Delta m_{15}$  of the supernova. Astronomers believe that the brightness of the supernova is driven by the amount of  $^{56}{\rm Ni}$  decayed. Thus, the more  $^{56}{\rm Ni}$  decayed, the brighter the supernovae. The models used in Kasen & Woosley (2007) demonstrated how the peak brightness and the  $\Delta m_{15}$  of the supernova changed with  $M_{\rm Ni}$ . These models were also designed to follow the Phillips' relation. Using the values of  $M_{\rm Ni}$  and  $\Delta m_{15}$  listed in Kasen & Woosley (2007), I interpolated the  $M_{\rm Ni}$  the supernovae in my sample would have had based on the  $\Delta m_{15}$  values. After I did that, I plotted the  $M_{\rm Ni}$  vs.  $\log\left(\frac{\rm O}{\rm H}\right)+12$  and ran the Spearman correlation test. With  $\rho=-0.36$ , the test indicated that there is no significant correlation between the  $M_{\rm Ni}$  and  $\log\left(\frac{\rm O}{\rm H}\right)+12$  at the 95% confidence level.

The lack of significant relationships within the above tests indicate that the metallicity of the galaxy, and by extension, the progenitor, is not a strong parameter in the peak brightness of the supernova.

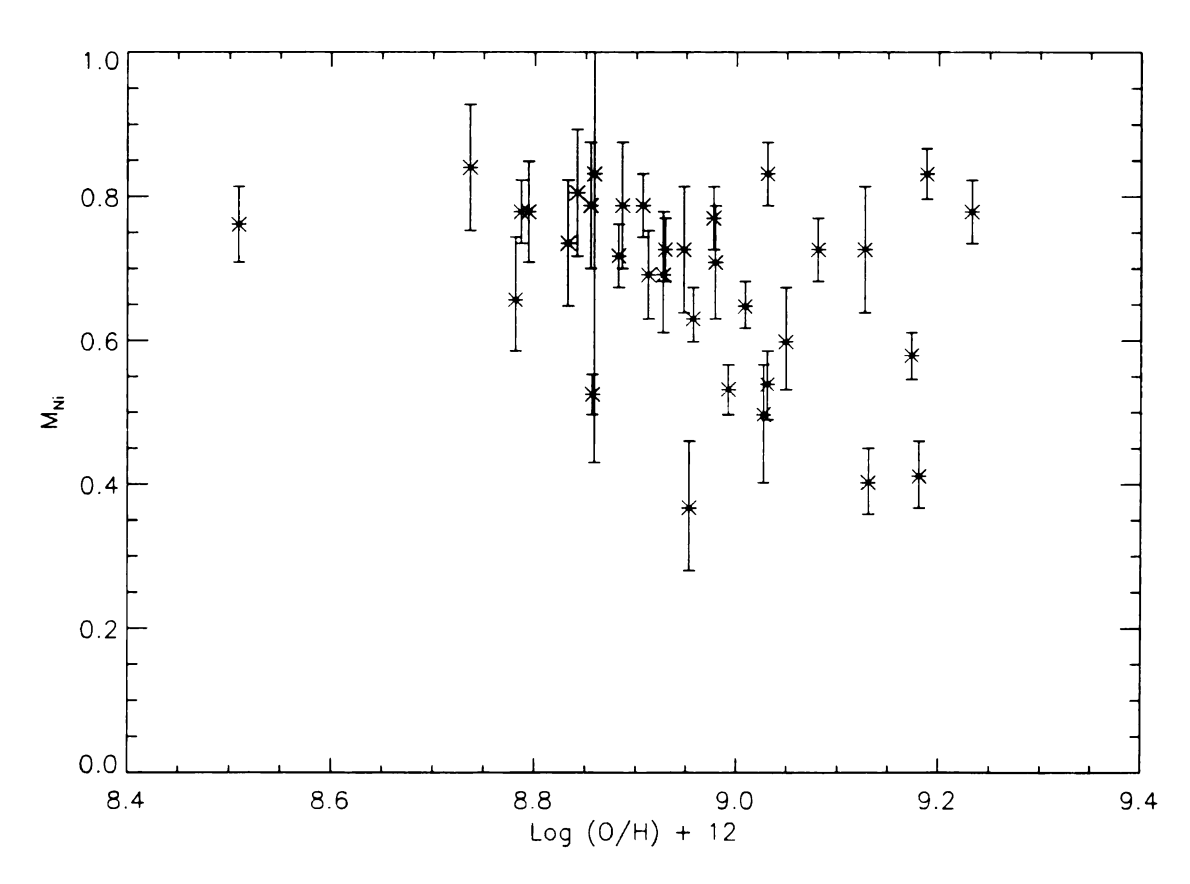


Figure 3.3: The mass of nickel in the progenitor  $(M_{\rm Ni})$  vs. the metallicity of the host galaxy  $(\log\left(\frac{\rm O}{\rm H}\right)+12)$ . A Spearman correlation test indicated that there is no significant correlation between  $M_{\rm Ni}$  and  $\log\left(\frac{\rm O}{\rm H}\right)+12$ .

## Chapter 4

## **Contemporary Studies**

#### 4.1 Metallicity Effects

As can be seen, the metallicity of the host galaxy, and thus the progenitor by extension, has no correlation with the brightness of the supernova. One explanation is that the effects from the metallicity are masked by the electron captures from the nuclear reactions in the progenitor. Chamulak et al. (2008) and Piro & Bildsten (2008) show that the electron abundance  $Y_e$  in the progenitor depends on the amount of  $^{12}$ C consumed during a long simmering phase prior to ignition. During this simmering phase,  $^{12}$ C is consumed via the reactions  $^{12}$ C( $^{12}$ C,  $\alpha$ ) $^{20}$ Ne and  $^{12}$ C( $^{12}$ C, p) $^{23}$ Na. Electron captures onto  $^{13}$ N and  $^{23}$ Na via the reactions  $^{12}$ C( $^{12}$ C, p) $^{13}$ N( $e^-$ ,  $p_e$ ) $^{13}$ C and  $^{23}$ Na( $e^-$ ,  $p_e$ ) $^{23}$ Ne, at density  $\rho = 3 \times 10^9 {\rm g \, cm}^{-3}$ , reduce  $Y_e$ . This reduction in  $Y_e$  leads to a decrease in the amount of  $^{56}$ Ni and increases the amount of  $^{54}$ Fe and  $^{58}$ Ni synthesized during the explosion (Brachwitz et al., 2000; Timmes et al., 2003). Thus, since the reduction in  $Y_e$  due to electron captures during simmering is greater than the change due to initial white dwarf composition for metallicity  $Z \lesssim Z_{\odot}$ , any correlation between host galaxy metallicity and SNe Ia peak luminosity will be

#### 4.2 Two-Component Model

Many astronomers now believe that the differences in the peak brightnesses of SNe Ia are due to the progenitors having two populations, and not the differences in the metallicities of the progenitors. Based on lower redshift data, Scannapieco & Bildsten (2005) and Mannucci et al. (2005, 2006) proposed that the disparity of the observed supernovae is caused by two components: one compontent that traces the star formation rate of the host galaxy, and a component that traces the total mass of the host galaxy. The component that traces the star-formation rate would account for the brighter supernovae only seen in active galaxies, while the component that traces the total mass would account for the dimmer supernovae mostly seen in passive galaxies. Using higher redshift (z < 0.75) data from Supernova Legacy Survey (SNLS), Sullivan et al. (2006) also found that the two component model described the observed SNe Ia rate well. However, Dahlen et al. (2004, 2008) and Strolger et al. (2004), using even higher redshift (z < 1.6) data from the Advanced Camera for Surveys (ACS) on the Hubble Space Telescope (HST), found that the two component model does not sufficiently predict the number of SNe Ia discovered at the higher z.

#### 4.2.1 Evidence for the Two-Component Model

The basis for the two-component model arises from strong empirical evidence. Mannucci et al. (2005) measured the SN rate per unit mass in the local universe. They found that the rate of SNe Ia very strongly depended on the (B-K) color of the host galaxy: blue galaxies (i.e., galaxies with on-going star formation) exhibited a larger rate of SNe Ia per unit mass than red galaxies (i.e., galaxies with little-to-no ongoing star formation) by a factor of  $\sim 30$ . This result indicates that the delay time (time between progenitor formation and supernova) must have a wide distribution: in star-forming galaxies, the delay time must be short, while in galaxies without star formation, the delay time must be much longer. As a result, Mannucci et al. (2005) proposed that two populations of progenitors exist: one related to the young stellar population, with the SNe Ia rate proportional to the star formation rate of the host galaxy, while the other is related to the older stellar population, with the SNe Ia rate proportional to the total stellar mass. In a later study, Mannucci et al. (2006) estimated that for the "prompt"-component, which traces the star formation rate and tends to be brighter,  $\sim 10^8$  years elapse between progenitor formation and ignition, and for the "tardy"-component, which traces the total mass and tends to be dimmer,  $\sim 3$  Gyr elapse between progenitor formation and ignition. Furthermore, based on their models, Mannucci et al. (2006) show that the "prompt"-component would dominate at z > 1.3 because of an increase in the star-formation rate, while the "tardy"-component would dominate at z < 1.3.

When adopting their model, Scannapieco & Bildsten (2005) followed Mannucci et al. (2005) and assumed that the SNe Ia rate is the sum of two components: a term proportional to the total stellar mass,  $M_*(t)$  and a term proportional to the instantaneous star formation rate  $\dot{M}_*(t)$ ,

$$\frac{SNR_{Ia}(t)}{(100 \text{ yr})^{-1}} = A \left[ \frac{M_{\star}(t)}{10^{10} M_{\odot}} \right] + B \left[ \frac{\dot{M}_{\star}(t)}{10^{10} M_{\odot} \text{ Gyr}^{-1}} \right]$$
(4.1)

where A and B are dimensionless quatities that are fixed with observations. A is dominant in older stellar populations, while B is dominant in younger stellar populations. This model is dominated by the prompt component, but allows for

significant numbers of SNe Ia to occur at later times. Also, with  $A = 4.4^{+1.6}_{-1.4} \times 10^{-2}$  and  $B = 2.6 \pm 1.1$ , this model produces the observed cosmic SNe Ia rate to  $z \le 1$ , including observations of galaxies with little-to-no star formation.

This model was also able to predict the Fe and O abundances observed at different redshifts. Since galaxy clusters are dominated by elliptical galaxies, previous models would combine the observed SNe Ia rate in elliptical galaxies with the total stellar mass in a cluster when creating models that estimated the amount of iron (Renzini et al., 1993). However, these models would underestimate the Fe content by an order of magnitude. On the other hand, Scannapieco & Bildsten (2005) assumed that the dominant source of Fe is from the prompt component, and not the late-time SNe Ia contribution as expected from elliptical galaxies. This resulted in [Fe/H] values that are roughly consistent with observations and are approximately an order of magnitude higher than previous estimates. This model also predicts the observed lack of [Fe/H] evolution with redshift (Tozzi et al., 2003). This lack of evolution does not appear in models dominated by late-time SNe Ia. Furthermore, Scannapieco & Bildsten (2005) looked at the relationship between SNe Ia and core-collapse SNe at short times and the amount of Fe and O, which is primarily synthesized in core-collapse SNe, produced. In their model, the overall SNe Ia Fe contribution as compared to core-collapse SNe is nearly 3 to 1, which means that the [O/Fe] should drop by a factor of 3, which is observed.

Sullivan et al. (2006) used SNLS data at 0.2 < z < 0.75 and found that the supernova rate was fitted well by the two-component model. SNLS uses several filters when repeatedly imaging the sky. This allows for highly precise lightcurves of detected supernovae and prompt spectroscopic followup of detected supernovae. Using these data, Sullivan et al. (2006) found that the SNe Ia rate per unit stellar mass is a strong function of the host galaxy star formation rate. Galaxies with

high star formation hosted  $\sim 10$  times as many SNe Ia as galaxies with zero star formation, which agrees with the findings of Mannucci et al. (2005). Also, Sullivan et al. (2006) found that galaxies with a higher star formation rate hosted more SNe Ia per unit mass than galaxies with a lower star formation rate. Like Scannapieco & Bildsten (2005), Sullivan et al. (2006) also found that the SNe Ia rate  $SNR_{Ia}$  is well represented by  $SNR_{Ia}(t) = AM(t) + B\dot{M}(t)$ , where the constants A is  $SNR_{Ia}$  per unit mass and B is the  $SNR_{Ia}$  per unit star formation, and M(t) is the total mass and  $\dot{M}(t)$  is the star formation rate. In addition to calculating the SNe Ia rate, Sullivan et al. (2006) observed a correlation between lightcurve width and host galaxy. Like Hamuy et al. (2000) and Mannucci et al. (2005), who observed SNe Ia at lower z, Sullivan et al. (2006) observed that SNe Ia with broad lightcurves (brighter SNe Ia) are found exclusively in galaxies with on-going star formation, while galaxies with no star formation only host SNe Ia with narrow lightcurves (dimmer SNe Ia).

## 4.2.2 Evidence against the Two-Component Model

Dahlen et al. (2004) and Strolger et al. (2004) used HST/ACS data at 0.2 < z < 1.6. The data was gathered as a part of the Great Observatories Origins Deep Survey (GOODS) campaign. During this campaign, two fields of the sky were observed by HST/ACS during five epochs, with each epoch separated by  $\sim 45$  days. Images were taken of the areas with multiple pointings using several different filters so that color could be calculated. Based on these data, Dahlen et al. (2004) and Strolger et al. (2004) found that the two component model overestimated the number of supernovae that would be seen at  $z \sim 1.4$ . Instead, what they observed was that there was a significant increase in the SNe Ia rate from low z to  $z \sim 1$ , and found that the rate decreased in the redshift range  $1 \lesssim z \lesssim 1.6$ . They found that a single component model with a delay time of  $\tau \gtrsim 2$  Gyr better fit the data at high redshift.

The single-component model also matched the calculated SNe Ia rates from lower redshift surveys (e.g. see Hardin et al., 2000; Cappellaro et al., 1999).

In a follow up survey, Dahlen et al. (2008) reached similar conclusions. When looking at higher redshift data (0.2 < z < 1.8), Dahlen et al. (2008) still showed that the two-component model does not accurately predict the observed SNe Ia rate. Models such as Scannapieco & Bildsten (2005), where the SNe Ia rate is dominated by the "prompt" (star formation tracing) component, overpredicted the SNe Ia rate at z > 1. Instead, Dahlen et al. (2008) observed that the SNe Ia rate decreased at z > 1. With their new observations, Dahlen et al. (2008) found that a single component model with a delay time of  $\sim$  3.4 Gyr better matched their data. Like the previous survey, this model also matched the calculated SNe Ia rates from lower redshift surveys. However, two-component models where both components contribute equally to the SNe Ia rate, such as Mannucci et al. (2006) more closely matched the observations than the two-component models dominated by the "prompt" component, but not as well as Dahlen et al. (2008).

## 4.2.3 Differences between the SNLS and GOODS Surveys

Differences between the SNLS and GOODS surveys could affect the observations and thus the model used to explain the data. One difference is how the data is collected. The SNLS survey is a ground-based "rolling" survey, meaning that the telescope continually scans sections of the sky on a nightly basis. In this case, the survey scans four sections of the sky, each about one square degree in size. Observations are completed every 3-4 nights during dark time (around new moon) with different filters, allowing for the construction of high-quality multicolor lightcurves (Sullivan et al., 2006). On the other hand, the GOODS survey is a space-based "rolling" survey, but the fields are smaller in number and size and the time between

observations longer than the SNLS survey. The survey covers two fields within the Hubble Deep Field - North and the Chandra Deep Field - South with an effective area of  $\sim 150 \text{ arcmin}^2$ . The time between observations is  $\sim 45 \text{ days}$ . Like the SNLS survey, multiple images are taken with multiple filters (Dahlen et al., 2004, 2008).

With a larger effective field of view and shorter time between observations, the SNLS would be more likely to observe SNe Ia, especially dim ones. Since dim SNe Ia have lightcurves that decline much more quickly than brighter SNe Ia, the GOODS survey may not observe as many dim ones. However, Riess (2007) believes that the GOODS survey is not missing objects at higher redshift. No apparent bias against SNe Ia at z>1.4 exists since GOODS is detecting core-collapse SNe, which are intrinsically much dimmer than SNe Ia, at higher redshift. When conducting the survey, the GOODS team took into account the brightness and luminosity function of SNe Ia. Using this information, the team believes that they are detecting the majority of the SNe Ia that should exist at higher redshift at 50% and 90% confidence levels. Based on these observations, the GOODS team is not detecting the "prompt"-component that, according to Mannucci et al. (2005, 2006) and Scannapieco & Bildsten (2005), is supposed to trace star-formation rate, which dominates at higher redshift (Riess, 2007).

## 4.3 Future Studies

Further studies are needed to confirm the two-component model. These studies need to include surveys with large sample sizes that see the entire distribution of supernovae (ie, from the dimmest to the brightest) and are not biased by galaxy type. Also, the surveys need to be fast-acting in order to observe dimmer, fasterdeclining supernovae. The proposed Large Synoptic Survey Telescope (LSST)<sup>1</sup> is an example of such a survey. The LSST is a ground-based telescope that will take images of the entire sky over a three night period. This will allow for observations of the dimmer supernovae and no bias in galaxy type. Data from surveys such as the LSST can help determine the SNe Ia rate at various z, which in turn can confirm the two-component model.

Once the type of supernovae is confirmed, then follow-up surveys like the SNLS would allow for more detailed observations of the supernovae over longer periods of time. Data from the follow-surveys can help determine progenitor scenario of SNe Ia. Theoretically, evidence of the companion star would be apparent in late-time spectra due to the companion's envelope being mixed with the ejecta of the supernova. However, these would be at a lower velocity than the ejecta, thus would appear as narrower lines (Leonard, 2007). Higher resolution spectra would be necessary to detect the contributions from the companion star to the spectra of the supernova.

<sup>&</sup>lt;sup>1</sup>http://www.lsst.org/lsst\_home.shtml

**BIBLIOGRAPHY** 

## **BIBLIOGRAPHY**

Arnett, D. 1999, ArXiv Astrophysics e-prints

Arnett, W. D. 1982, ApJ, 253, 785

Astier, P., Guy, J., Regnault, N., Pain, R., Aubourg, E., Balam, D., Basa, S., Carlberg, R. G., Fabbro, S., Fouchez, D., Hook, I. M., Howell, D. A., Lafoux, H., Neill, J. D., Palanque-Delabrouille, N., Perrett, K., Pritchet, C. J., Rich, J., Sullivan, M., Taillet, R., Aldering, G., Antilogus, P., Arsenijevic, V., Balland, C., Baumont, S., Bronder, J., Courtois, H., Ellis, R. S., Filiol, M., Gonçalves, A. C., Goobar, A., Guide, D., Hardin, D., Lusset, V., Lidman, C., McMahon, R., Mouchet, M., Mourao, A., Perlmutter, S., Ripoche, P., Tao, C., & Walton, N. 2006, A&A, 447, 31

Barbon, R., Ciatti, F., & Rosino, L. 1973, A&A, 25, 241

Brachwitz, F., Dean, D. J., Hix, W. R., Iwamoto, K., Langanke, K., Martínez-Pinedo, G., Nomoto, K., Strayer, M. R., Thielemann, F.-K., & Umeda, H. 2000, ApJ, 536, 934

Branch, D. 1986, ApJ, 300, L51

—. 2001, PASP, 113, 169

Branch, D., Livio, M., Yungelson, L. R., Boffi, F. R., & Baron, E. 1995, PASP, 107, 1019

Branch, D. & Miller, D. L. 1993, ApJ, 405, L5

Cappellaro, E., Evans, R., & Turatto, M. 1999, A&A, 351, 459

Chamulak, D. A., Brown, E. F., Timmes, F. X., & Dupczak, K. 2008, ApJ, 677, 160

Colgate, S. A. 1979, ApJ, 232, 404

Colgate, S. A. & McKee, C. 1969, ApJ, 157, 623

Dahlen, T., Strolger, L.-G., & Riess, A. G. 2008, ArXiv e-prints, 803

- Dahlen, T., Strolger, L.-G., Riess, A. G., Mobasher, B., Chary, R.-R., Conselice,
  C. J., Ferguson, H. C., Fruchter, A. S., Giavalisco, M., Livio, M., Madau, P.,
  Panagia, N., & Tonry, J. L. 2004, ApJ, 613, 189
- Doggett, J. B. & Branch, D. 1985, AJ, 90, 2303
- Gallagher, J. S., Garnavich, P. M., Berlind, P., Challis, P., Jha, S., & Kirshner, R. P. 2005, ApJ, 634, 210
- Gaskell, C. M., Cappellaro, E., Dinerstein, H. L., Garnett, D. R., Harkness, R. P., & Wheeler, J. C. 1986, ApJ, 306, L77
- Goobar, A. & Perlmutter, S. 1995, ApJ, 450, 14
- Gutierrez, J., Garcia-Berro, E., Iben, I. J., Isern, J., Labay, J., & Canal, R. 1996, ApJ, 459, 701
- Hachinger, S., Mazzali, P. A., & Benetti, S. 2006, MNRAS, 370, 299
- Hamuy, M., Trager, S. C., Pinto, P. A., Phillips, M. M., Schommer, R. A., Ivanov, V., & Suntzeff, N. B. 2000, AJ, 120, 1479
- Hardin, D., Afonso, C., Alard, C., Albert, J. N., Amadon, A., Andersen, J., Ansari, R., Aubourg, É., Bareyre, P., Bauer, F., Beaulieu, J. P., Blanc, G., Bouquet, A., Char, S., Charlot, X., Couchot, F., Coutures, C., Derue, F., Ferlet, R., Glicenstein, J. F., Goldman, B., Gould, A., Graff, D., Gros, M., Haissinski, J., Hamilton, J. C., de Kat, J., Kim, A., Lasserre, T., Lesquoy, É., Loup, C., Magneville, C., Mansoux, B., Marquette, J. B., Maurice, É., Milsztajn, A., Moniez, M., Palanque-Delabrouille, N., Perdereau, O., Prévot, L., Regnault, N., Rich, J., Spiro, M., Vidal-Madjar, A., Vigroux, L., Zylberajch, S., & The EROS Collaboration. 2000, A&A, 362, 419
- Henry, R. B. C. & Worthey, G. 1999, PASP, 111, 919
- Hillebrandt, W. & Niemeyer, J. C. 2000, ARA&A, 38, 191
- Howell, D. A., Sullivan, M., Nugent, P. E., Ellis, R. S., Conley, A. J., Le Borgne, D.,
  Carlberg, R. G., Guy, J., Balam, D., Basa, S., Fouchez, D., Hook, I. M., Hsiao,
  E. Y., Neill, J. D., Pain, R., Perrett, K. M., & Pritchet, C. J. 2006, Nature, 443, 308
- Iben, Jr., I. & Tutukov, A. V. 1984, ApJS, 54, 335
- Kasen, D. 2006, ApJ, 649, 939
- Kasen, D. & Woosley, S. E. 2007, ApJ, 656, 661

Leibundgut, B., Kirshner, R. P., Phillips, M. M., Wells, L. A., Suntzeff, N. B., Hamuy, M., Schommer, R. A., Walker, A. R., Gonzalez, L., Ugarte, P., Williams, R. E., Williger, G., Gomez, M., Marzke, R., Schmidt, B. P., Whitney, B., Coldwell, N., Peters, J., Chaffee, F. H., Foltz, C. B., Rehner, D., Siciliano, L., Barnes, T. G., Cheng, K.-P., Hintzen, P. M. N., Kim, Y.-C., Maza, J., Parker, J. W., Porter, A. C., Schmidtke, P. C., & Sonneborn, G. 1993, AJ, 105, 301

Leonard, D. C. 2007, ApJ, 670, 1275

Mannucci, F., Della Valle, M., & Panagia, N. 2006, MNRAS, 370, 773

Mannucci, F., Della Valle, M., Panagia, N., Cappellaro, E., Cresci, G., Maiolino, R., Petrosian, A., & Turatto, M. 2005, A&A, 433, 807

Matteucci, F., Panagia, N., Pipino, A., Mannucci, F., Recchi, S., & Della Valle, M. 2006, MNRAS, 372, 265

Miyaji, S., Nomoto, K., Yokoi, K., & Sugimoto, D. 1980, PASJ, 32, 303

Nomoto, K. 1982, ApJ, 253, 798

Nomoto, K., Thielemann, F.-K., & Yokoi, K. 1984, ApJ, 286, 644

Nugent, P., Branch, D., Baron, E., Fisher, A., Vaughan, T., & Hauschildt, P. H. 1995, Phys. Rev. Lett., 75, 394

Perlmutter, S., Aldering, G., Goldhaber, G., Knop, R. A., Nugent, P., Castro, P. G.,
Deustua, S., Fabbro, S., Goobar, A., Groom, D. E., Hook, I. M., Kim, A. G.,
Kim, M. Y., Lee, J. C., Nunes, N. J., Pain, R., Pennypacker, C. R., Quimby, R.,
Lidman, C., Ellis, R. S., Irwin, M., McMahon, R. G., Ruiz-Lapuente, P., Walton,
N., Schaefer, B., Boyle, B. J., Filippenko, A. V., Matheson, T., Fruchter, A. S.,
Panagia, N., Newberg, H. J. M., Couch, W. J., & The Supernova Cosmology
Project. 1999, ApJ, 517, 565

Perlmutter, S., Gabi, S., Goldhaber, G., Goobar, A., Groom, D. E., Hook, I. M., Kim, A. G., Kim, M. Y., Lee, J. C., Pain, R., Pennypacker, C. R., Small, I. A., Ellis, R. S., McMahon, R. G., Boyle, B. J., Bunclark, P. S., Carter, D., Irwin, M. J., Glazebrook, K., Newberg, H. J. M., Filippenko, A. V., Matheson, T., Dopita, M., Couch, W. J., & The Supernova Cosmology Project. 1997, ApJ, 483, 565

Phillips, M. M. 1993, ApJ, 413, L105

Piersanti, L., Gagliardi, S., Iben, I. J., & Tornambé, A. 2003, ApJ, 583, 885

Pilyugin, L. S., Vílchez, J. M., & Contini, T. 2004, A&A, 425, 849

Piro, A. L. & Bildsten, L. 2008, ApJ, 673, 1009

Pskovskii, I. P. 1977, Soviet Astronomy, 21, 675

Pskovskii, Y. P. 1984, Soviet Astronomy, 28, 658

Reindl, B., Tammann, G. A., Sandage, A., & Saha, A. 2005, ApJ, 624, 532

Renzini, A., Ciotti, L., D'Ercole, A., & Pellegrini, S. 1993, ApJ, 419, 52

Riess, A. 2007, in Paths to Exploding Stars: Accretion and Eruption, Kavli Institute for Theoretical Physics

Riess, A. G., Press, W. H., & Kirshner, R. P. 1995, ApJ, 438, L17

Scannapieco, E. & Bildsten, L. 2005, ApJ, 629, L85

Strolger, L.-G., Riess, A. G., Dahlen, T., Livio, M., Panagia, N., Challis, P., Tonry, J. L., Filippenko, A. V., Chornock, R., Ferguson, H., Koekemoer, A., Mobasher, B., Dickinson, M., Giavalisco, M., Casertano, S., Hook, R., Blondin, S., Leibundgut, B., Nonino, M., Rosati, P., Spinrad, H., Steidel, C. C., Stern, D., Garnavich, P. M., Matheson, T., Grogin, N., Hornschemeier, A., Kretchmer, C., Laidler, V. G., Lee, K., Lucas, R., de Mello, D., Moustakas, L. A., Ravindranath, S., Richardson, M., & Taylor, E. 2004, ApJ, 613, 200

Sullivan, M., Le Borgne, D., Pritchet, C. J., Hodsman, A., Neill, J. D., Howell, D. A., Carlberg, R. G., Astier, P., Aubourg, E., Balam, D., Basa, S., Conley, A., Fabbro, S., Fouchez, D., Guy, J., Hook, I., Pain, R., Palanque-Delabrouille, N., Perrett, K., Regnault, N., Rich, J., Taillet, R., Baumont, S., Bronder, J., Ellis, R. S., Filiol, M., Lusset, V., Perlmutter, S., Ripoche, P., & Tao, C. 2006, ApJ, 648, 868

Taam, R. E. 1980, ApJ, 242, 749

Tegmark, M., Strauss, M. A., Blanton, M. R., Abazajian, K., Dodelson, S., Sandvik, H., Wang, X., Weinberg, D. H., Zehavi, I., Bahcall, N. A., Hoyle, F., Schlegel, D., Scoccimarro, R., Vogeley, M. S., Berlind, A., Budavari, T., Connolly, A., Eisenstein, D. J., Finkbeiner, D., Frieman, J. A., Gunn, J. E., Hui, L., Jain, B., Johnston, D., Kent, S., Lin, H., Nakajima, R., Nichol, R. C., Ostriker, J. P., Pope, A., Scranton, R., Seljak, U., Sheth, R. K., Stebbins, A., Szalay, A. S., Szapudi, I., Xu, Y., Annis, J., Brinkmann, J., Burles, S., Castander, F. J., Csabai, I., Loveday, J., Doi, M., Fukugita, M., Gillespie, B., Hennessy, G., Hogg, D. W., Ivezić, Ž., Knapp, G. R., Lamb, D. Q., Lee, B. C., Lupton, R. H., McKay, T. A., Kunszt, P., Munn, J. A., O'Connell, L., Peoples, J., Pier, J. R., Richmond, M., Rockosi, C., Schneider, D. P., Stoughton, C., Tucker, D. L., vanden Berk, D. E., Yanny, B., & York, D. G. 2004, Phys. Rev. D, 69, 103501

Timmes, F. X., Brown, E. F., & Truran, J. W. 2003, ApJ, 590, L83

Tozzi, P., Rosati, P., Ettori, S., Borgani, S., Mainieri, V., & Norman, C. 2003, ApJ, 593, 705

Tremonti, C. A., Heckman, T. M., Kauffmann, G., Brinchmann, J., Charlot, S., White, S. D. M., Seibert, M., Peng, E. W., Schlegel, D. J., Uomoto, A., Fukugita, M., & Brinkmann, J. 2004, ApJ, 613, 898

Turatto, M., Cappellaro, E., & Benetti, S. 1994, AJ, 108, 202

van Dyk, S. D. 1992, AJ, 103, 1788

Woosley, S. E., Kasen, D., Blinnikov, S., & Sorokina, E. 2007, ApJ, 662, 487

Woosley, S. E., Taam, R. E., & Weaver, T. A. 1986, ApJ, 301, 601

